Atmósfera 38, 1-21 (2024)
https://doi.org/10.20937/ATM.53181

Development and evaluation of a bulk three-moment parameterization scheme incorporating the processes of sedimentation and collision-coalescence

Lainer DONET[1]* and Lester ALFONSO[2]

[1] *Instituto de Ciencias de la Atmósfera y Cambio Climático, Universidad Nacional Autónoma de México, Circuito de la Investigación Científica s/n, Ciudad Universitaria, 04510 Ciudad de México, México.*
[2] *Colegio de Ciencia y Tecnología, Universidad Autónoma de la Ciudad de México, Prol. San Isidro 151, San Lorenzo Tezonco, 09790 Ciudad de México, México.*
*Corresponding author; email: lainer.donet@atmosfera.unam.mx

Received: March 23, 2022; Accepted: August 30, 2022

RESUMEN

Hay pocos modelos microfísicos de tres momentos que consideren otros procesos además de la sedimentación. Por lo tanto, una evaluación del desempeño de este tipo de esquemas bajo la acción combinada de los procesos de sedimentación y colisión-coalescencia es un tema de interés. En este estudio se desarrolló y posteriormente se evaluó un esquema parametrizado de tres momentos para nubes calientes a través de su comparación con un modelo de microfísica detallada. Para evaluar el impacto de la sedimentación y el efecto combinado de la sedimentación y la colisión-coalescencia en la distribución por tamaños de las gotas (DSD, por su sigla en inglés), se realizaron corridas con un modelo cinemático para diferentes DSD con diferentes valores iniciales del parámetro de forma. Para la sedimentación pura se obtuvo una buena correspondencia entre el esquema de tres momentos y el modelo explícito, con una coincidencia prácticamente perfecta de cantidades unitarias para valores mayores del parámetro de la forma inicial de la distribución gamma. En general, se demostró que la parametrización de tres momentos funciona mucho mejor que el esquema de dos momentos. Las simulaciones realizadas para este caso confirman (como se reportó en estudios anteriores) que, para la sedimentación pura, los esquemas de tres momentos brindan una representación más completa de la evolución de la distribución por tamaños. También se evaluó el impacto del efecto combinado de los procesos de sedimentación y colisión-coalescencia en la distribución por tamaños. Se pudo observar que hay ciertas diferencias entre el esquema parametrizado y el modelo espectral cuando se incorpora el proceso de colisión de coalescencia, ya que el inicio de la precipitación ocurre antes en el esquema parametrizado de tres momentos. Se puede concluir que el esquema microfísico de tres momentos es capaz de reproducir en términos generales los resultados del modelo de microfísica explícita.

ABSTRACT

There are a few three-moment schemes that consider other processes besides sedimentation. Thus, a performance assessment of these types of schemes due to the combined effect of sedimentation and other microphysical processes is a matter of interest. In this study, a warm rain bulk three-moment parameterized scheme was developed and evaluated through a detailed comparison with a bin microphysical scheme. To evaluate the impact of sedimentation and the combined effect of sedimentation and collision-coalescence on the droplet size distribution (DSD), a rain shaft model was applied to the DSD with different initial values of the shape parameter. For pure sedimentation, a good correspondence was obtained between the three-moment scheme and the explicit model, with a practically perfect coincidence of bulk quantities for larger values of the gamma distribution's initial shape parameter and, in general, the three-moment parameterization scheme performing much better than the two-moment scheme. The simulations performed for this case confirm (as reported in previous studies) that for pure sedimentation, the three-moment parameterization schemes deliver a physically more complete representation of the evolution of droplet size distribution. The impact of the combined effect of sedimentation and collision-coalescence processes on DSD was also assessed. We could observe that certain differences arise between the parameterized scheme and the spectral model when the collision-coalescence process is incorporated, as the onset of precipitation occurs earlier in the three-moment parameterized scheme. It can be concluded that, in general, the three-moment warm rain bulk microphysics scheme is able to reproduce the results of the reference bin microphysical model.

Keywords: cloud microphysics, method of moments, parameterizations.

1. Introduction

Bulk microphysical schemes are widely used to model cloud microphysical processes. For bulk parameterizations, the droplet size distribution (DSD) of each hydrometeor category is approximated by a continuous function for which there are one or more free parameters. Usually, from the DSD one or more prognostic moments can be calculated, for which predictive equations for microphysical processes are computed.

Initially, bulk schemes (Kessler, 1969) incorporated only a single moment (usually the third moment regarding the diameter of the DSD, proportional to the liquid water content). As the complexity of the models increased, the zeroth moment with respect to the drop diameter (which is equal to the total number concentration) was incorporated in two-moment bulk schemes (e.g., Murakami, 1990; Ferrier 1994; Reisner et al., 1998; Seifert and Beheng, 2001; Morrison et al., 2005; Cohard and Pinty, 2000).

For parameterized microphysics (e.g., Khain et al., 2015; Milbrandt and Yau, 2005a; Seifert and Beheng, 2006; Morrison et al., 2009; Lim and Hong, 2010), a gamma distribution is usually assumed for the drop size distribution:

$$N(D) = n_0 D^{\mu} e^{-\lambda D} \tag{1}$$

where D is drop diameter (in cm), n_0 is the intercept of the distribution (in cm^{-4}), μ is the shape parameter (non-dimensional) and λ is the slope parameter (in cm^{-1}). The moments of order 0 and order 3 with respect to radius or diameter (which are equal and proportional to the concentration and the liquid water content respectively) are usually predicted.

By fixing the shape parameter μ, the computational burden of the bulk approach is drastically reduced, but other drawbacks arise. For example, while calculating the sedimentation some authors reported an excess sorting (e.g., Wacker and Seifert, 2001; Milbrandt and McTaggart-Cowan, 2010; Shipway and Hill, 2012).

Size sorting can be observed in a polydisperse population of droplets, due to the fact that larger drops have larger terminal velocities and settle much more quickly, resulting in a spatial separation of droplets. It can be modeled in two-moment schemes, as M_3 sediments much faster than M_0. However, when fixing μ, there is an over-prediction of M_3, and an under-prediction of M_0 (when comparing with an explicit reference model) generating the excess size sorting reported by some authors.

For a scheme with a fixed value of μ, the excess sorting occurs due to the fact that the ratio of the moment-weighted sedimentation velocities (V_k/V_j, with $k > j$), which is a function of the shape parameter, is always positive and larger than 1 (Milbrandt and McTaggart-Cowan, 2010). Therefore, M_k has always larger sedimentation rates than M_j. Then, as the ratio M_3/M_0 increases, the mean radius will also increase at the lower edge of the sedimentation profile. This behavior is a consequence of assuming a constant value of μ and, implicitly, a prescribed constant ratio of the bulk fall velocities.

For two-moment schemes, this problem can be mitigated by using a fixed but large value of μ, consequently obtaining moment-weighted fall velocities for M_3 and M_0 closer in value. An alternative solution (without changing μ) is to make the ratio V_k/V_j closer to 1 by increasing V_j. However, these are only palliatives as the mean radius will always increase at the leading edge of the sedimentation profile. Milbrandt and Yau (2005a) proposed a diagnosing relationship for the shape parameter as a function of the mean droplet diameter $\mu = f(D_m)$ to control the size sorting. Also, in a more general approach, the shape parameter was parameterized as a function of M_3 and M_0. Additionally, diagnosing relationships were extracted from bin microphysical models by fitting the explicit droplet size distributions to gamma distributions in order to calculate the shape parameter.

Three-moment parameterization schemes were introduced in order to obtain a more physically based representation of the droplet size distribution evolution. For these schemes, an additional moment (commonly the sixth moment, M_6, which is proportional to the radar reflectivity) is added in order to calculate the shape parameter μ. As a result, they are more able to approximate the bin reference models for pure sedimentation (Milbrandt and Yau, 2005a). For the sedimentation process, three-moment parameterization schemes performed better than two-moment schemes, because they predict a larger reflectivity-weighted fall velocity than the mass-weighted fall speed, resulting in a larger sedimentation rate for M_6. As a result, there is an increase in the shape parameter μ during size sorting and, consequently, the droplet size distribution narrows, thus further limiting the size sorting as the weighted-fall speeds for the different moments are closer. This feedback is the reason for three-moment schemes that provide a more realistic description of the sedimentation process (Dawson et al., 2014).

There are few three-moment schemes that consider other processes besides sedimentation (Szyrmer et al., 2005; Shipway and Hill, 2012; Dawson et al., 2014; Loftus et al., 2014; Naumann and Seifert, 2016). In Naumann and Seifert (2016), a three-moment rain scheme that includes the processes of sedimentation, evaporation, and collision-coalescence, was compared with a Lagrangian model obtaining a good correspondence between the bulk and the explicit models. Paukert et al. (2019) developed a three-moment scheme that included various microphysical processes, such as sedimentation, evaporation, self-collection, and collisional breakup.

The aim of this study is to advance further in this direction through the development and assessment of a three-moment microphysical scheme that includes the processes of sedimentation and collision-coalescence. To quantify the impact of these processes on drop size distribution and shape parameter evolution, simulations were performed varying the shape parameter of the initial distribution. The results obtained with the three-moment microphysical scheme are in good agreement with the explicit Eulerian reference model. It was found that the collision-coalescence process counteracts the sedimentation tendency to create narrow droplet size distributions.

The paper is organized as follows: section 2 presents the three-moment parameterization scheme. The numerical implementation of the sedimentation model for both the bulk and the explicit schemes is presented in section 3. Section 4 is devoted to the analysis of simulation results. Concluding remarks are given in section 5.

2. The bulk three-moment parameterization scheme

2.1 Obtaining the droplet size distribution shape as a function of moments

The three-parameter gamma distribution function (Eq. 1) has been widely used in bulk parameterization schemes (e.g., Seifert and Beheng, 2001; Milbrandt and Yau, 2005b; Morrison et al., 2005; Milbrandt and McTaggart-Cowan, 2010; Ziemer and Wacker, 2014). The parameters n_0 and λ must be positive, while μ can also be negative. From distribution parameters, the value of any moment $M_{(i)}$ can be computed analytically from the expression:

$$M_{(i)} = \int_0^\infty D^i N(D) dD = n_0 \Gamma\left(i + \mu + 1\right) \lambda^{-(i+\mu+1)} \tag{2}$$

The main objective of a three-moment parameterization scheme is to obtain the three parameters of the gamma distribution (Eq. [1]) from the prognostic moments. The intersection n_0 and the scale parameter λ of the distribution in Eq. (1) are calculated from the moments M_0 and M_3 by using Eqs (3) and (4) (Milbrandt and MacTaggart-Cowan, 2010):

$$n_0 = \left[\frac{M_j}{\Gamma\left(j+\mu+1\right)}\right]^{(k+\mu+1)/(k-j)} \times \left[\frac{M_k}{\Gamma\left(k+\mu+1\right)}\right]^{-(j+\mu+1)/(k-j)} \tag{3}$$

$$\lambda = \left[\frac{n_0 \Gamma\left(j+\mu+1\right)}{M_j}\right]^{1/(j+\mu+1)} \tag{4}$$

and the shape parameter μ is obtained from the solution of the cubic equation (Paukert et al., 2019):

$$\mu^3 + c_1\mu^2 + c_2\mu + c_3 = 0 \tag{5}$$

where $c_1 = \dfrac{15-6K}{1-K}$; $c_1 = \dfrac{74-11K}{1-K}$;

$$c_3 = \frac{120-6K}{1-K} \quad \text{and} \quad K = \frac{M_0 M_6}{M_3^2}$$

Following Paukert et al. (2019), we set $\mu = 0$ for $K > 20$, and $\mu = 20$ for $K < 1.46$; then $\mu \in [0, 20]$. For $K \in [1.46, 20]$. the equation can be solved either analytically by using Cardano's formula (Press et al., 1992) or numerically. At each time step, in order to calculate the three parameters, the prognostic moments need first to be updated due to microphysical processes (sedimentation and collision-coalescence). Then, the new parameters of the distribution are calculated from Eqs. (2)-(5).

2.2 Updating the moments due to collision-coalescence process

Within the bulk approach, the DSD is decomposed in two parts. Drops smaller that a threshold radius, that is typically within a range from 20 μm (Khairoutdinov and Kogan, 2000; Wood and Blossey, 2005) to 41 μm (Cohard and Pinty, 2000; Beheng, 2010), are called cloud droplets, and larger droplets are called raindrops. In this paper, a threshold diameter of $D = 82$ μm was adopted following Cohard and Pinty (2000).

The following interactions between cloud droplets and raindrops, due to collision-coalescence, are assumed: cloud droplet-cloud droplet collisions, cloud droplet-raindrop collisions, and raindrop-raindrop collisions (Lee and Baik, 2017). For cloud droplet-cloud droplet interactions, two processes can be identified: autoconversion (if the resulting drop is a raindrop) and self-collection (if the formed drop is a cloud droplet). For cloud droplet-raindrop interactions and raindrop-raindrop collisions, the accretion and the self-collection processes can be identified. For both these latter processes, the result is a raindrop.

The tendencies for the number concentration, mass mixing ratio and radar reflectivity for both cloud droplets (N_c, Q_c, Z_c) and raindrops(N_r, Q_r, Z_r) due to autoconversion, accretion and self-collection are:

$$\frac{\partial N_c}{\partial t} = \left.\frac{\partial N_c}{\partial t}\right|_{auto} + \left.\frac{\partial N_c}{\partial t}\right|_{acc} + \left.\frac{\partial N_c}{\partial t}\right|_{selfcoll} \tag{6}$$

$$\frac{\partial Q_c}{\partial t} = \left.\frac{\partial Q_c}{\partial t}\right|_{auto} + \left.\frac{\partial Q_c}{\partial t}\right|_{acc} \tag{7}$$

$$\frac{\partial Z_c}{\partial t} = \left.\frac{\partial Z_c}{\partial t}\right|_{aut} + \left.\frac{\partial Z_c}{\partial t}\right|_{acc} + \left.\frac{\partial Z_c}{\partial t}\right|_{selfcoll} \tag{8}$$

$$\frac{\partial N_r}{\partial t} = \left.\frac{\partial N_r}{\partial t}\right|_{auto} + \left.\frac{\partial N_r}{\partial t}\right|_{selfcoll} \tag{9}$$

$$\frac{\partial Q_r}{\partial t} = \left.\frac{\partial Q_r}{\partial t}\right|_{auto} + \left.\frac{\partial Q_r}{\partial t}\right|_{acc} \tag{10}$$

$$\frac{\partial Z_r}{\partial t} = \left.\frac{\partial Z_r}{\partial t}\right|_{auto} + \left.\frac{\partial Z_r}{\partial t}\right|_{acc} + \left.\frac{\partial Z_r}{\partial t}\right|_{selfcoll} \tag{11}$$

The moment tendencies are calculated from the former equations by noticing that $N_{iT} = M_{i0}$, $LWC = (6/\mu\rho_L)M_3$ and $Z_i = M_{i6}$. The equations for each process are described in detail in section S1 of the supplementary material. The changes of the reflectivity due to microphysical processes (autoconversion, accretion and self-collection) are calculated following Milbrandt and Yau (2005b), and only Type 1 tendency equations are considered. Type 2 and Type 3 tendencies are not considered in our model, as Type 2 tendencies represent changes in radar reflectivity when a new hydrometeor is initiated, and Type 3 tendencies represent conversion from one hydrometeor category to another (Milbrandt and Yau, 2005b). Type 1 tendency equations for the radar reflectivity can be obtained by taking the derivative of Eq. (12), considering that the shape parameter μ_i is constant.

$$Z_i = M_{i6} = \frac{G(\mu_i)}{c_i^2}\frac{(\rho_a Q_i)^2}{N_{Ti}} \tag{12}$$

$$G(\mu_i) = \frac{(6+\mu_i)(5+\mu_i)(4+\mu_i)}{(3+\mu_i)(2+\mu_i)(1+\mu_i)} \tag{13}$$

In Eqs. (12) and (13), i stands again for cloud or rain, $c_i = \rho_i\,(\mu/6)$, and ρ_a is the density of air. Then, the reflectivity rates due to autoconversion, accretion and self-collection are calculated from the equations (Milbrandt and Yau, 2005b):

$$\left.\frac{dZ_c}{dt}\right|_{auto} = \frac{G(\mu_i)}{c_c^2}\rho_a^{\ 2} \left[2\frac{Q_c}{N_c}\left.\frac{dQ_c}{dt}\right|_{auto} - \left(\frac{Q_c}{N_c}\right)^2 \left.\frac{dN_c}{dt}\right|_{auto}\right] \tag{14}$$

$$\left.\frac{dZ_c}{dt}\right|_{accre} = \frac{G(\mu_i)}{c_c^2}\rho_a{}^2 \left[2\frac{Q_c}{N_c}\left.\frac{dQ_c}{dt}\right|_{accre} - \left(\frac{Q_c}{N_c}\right)^2 \left.\frac{dN_c}{dt}\right|_{accre}\right] \tag{15}$$

$$\left.\frac{dZ_r}{dt}\right|_{accre} = \frac{G(\mu_i)}{c_r^2}\rho_a{}^2 \left[2\frac{Q_r}{N_r}\left.\frac{dQ_r}{dt}\right|_{accre} - \left(\frac{Q_r}{N_r}\right)^2 \left.\frac{dN_r}{dt}\right|_{accre}\right] \tag{16}$$

$$\left.\frac{dZ_c}{dt}\right|_{selfcoll} = \frac{G(\mu_i)}{c_c^2}\rho_a{}^2 \left[2\frac{Q_c}{N_c}\left.\frac{dQ_c}{dt}\right|_{selfcoll} - \left(\frac{Q_c}{N_c}\right)^2 \left.\frac{dN_c}{dt}\right|_{selfcoll}\right] \tag{17}$$

$$\left.\frac{dZ_r}{dt}\right|_{selfcoll} = \frac{G(\mu_i)}{c_r^2}\rho_a{}^2 \left[2\frac{Q_r}{N_r}\left.\frac{dQ_r}{dt}\right|_{selfcoll} - \left(\frac{Q_r}{N_r}\right)^2 \left.\frac{dN_r}{dt}\right|_{selfcoll}\right] \tag{18}$$

$$\left.\frac{dZ_r}{dt}\right|_{auto} = -\left.\frac{dZ_c}{dt}\right|_{auto} \tag{19}$$

2.3 Implementation of the bulk model for sedimentation

For the sedimentation process, the parameterized microphysics consists of a system of three budget equations for each moment of the DSD:

$$\left.\frac{\partial M_k}{\partial t}\right|_{sedi} = \frac{\partial (M_k V_k)}{\partial z} \tag{20}$$

where M_k is the moment of the DSD, k is the order of the moment ($k = 0.3$ and 6 with respect to the drop diameter) and V_k is the moment-weighted sedimentation velocity that is calculated from the equation:

$$V_k = a\left(\frac{\rho_0}{\rho}\right)^b \frac{\Gamma(k+\mu+b+1)}{\Gamma(k+\mu+1)}\lambda^{-b} \tag{21}$$

In Eq. (21) Γ is the gamma function, and λ and μ are the slope and the shape parameter of the gamma distribution, respectively. For the numerical solution of Eq. (20), 80 vertical layers with Δz = 100m were defined. All equations are integrated in time by using a first-order Euler forward-scheme with a time step of Δt = 1s.

3. The bin microphysics reference model and methodology of comparison with the bulk microphysics scheme

3.1 The bin microphysics reference model

The spectral bin model, which is used as a reference, solves the partial differential equation:

$$\frac{\partial f(z,t,D)}{\partial t} = \frac{\partial \left(f(z,t,D)V(D)\right)}{\partial z} + \left(\frac{\partial f(z,t,D)}{\partial t}\right)_{coagulation} \tag{22}$$

where f(z, t, D) is the DSD (as a function of height z, time and droplet diameter D), $V(D)$ is the terminal velocity, and $(\partial f(z, D)/\partial t)|_{coagulation}$ is the source term due to the coagulation process defined by the kinetic collection equation (KCE). This equation, in its formulation for a size distribution *f(x, t)* with drop mass x (Pruppacher and Klett, 1997) has the form:

$$\frac{\partial f(x,t)}{\partial t} = \frac{1}{2}\int_0^x f(x-y,t)f(y,t)K(x-y,y)dy - f(x,t)\int_0^\infty f(y,t)K(x,y)dy \tag{23}$$

where $K(x, y)$ is the hydrodynamic kernel, which is a symmetric function of the mass of the colliding droplets

$$K(x,y) = \pi (r_x + r_y)^2 \left|V(x) - V(y)\right| E(r_x, r_y) \tag{24}$$

where r_x and r_y are the radii of droplets with masses x and y, respectively, and $E(r_x,r_y)$ are the Hall (1980) collection efficiencies. The KCE was solved using the flux method developed by Bott (1998), and a drop size range from 1 to 2500 μm was used during the simulations. The size distribution *f(x)* was defined the same as in Bott (1998) and Berry (1967), and is represented by 33 mass doubling categories, then mass m_k in the category k is determined as $m_k = 2m_{k-1}$.

The terminal velocity $V(D)$ in Eq. (24) is given as a power-law relationship (Straka, 2009):

$$V(D) = a\left(\frac{\rho_0}{\rho}\right)^b D^b \tag{25}$$

where a = 1300 $cm^{0.5}s^{-1}$, b=0.5 (Gunn and Kinzer, 1949) and (ρ_0/ρ) is the air density correction factor (with ρ and ρ_0 denoting the air density aloft and at the surface, respectively) that, for simplicity, is assumed to be 1 throughout this study. For the numerical solution of Eq. (22), a forward-in-time and upstream-in-space method was implemented with a time step of Δt = 1 s. The value of b is the same for Eqs. (21) and (25).

3.2 Methodology of comparison with the bulk microphysics scheme

As the size distribution *f(x)* for the bin microphysical model was defined the same as in Bott (1998), it has to be initialized from the condition (Berry, 1967)

$$f(x)dx = N(D)dD \tag{26}$$

Then, given a three-parameter gamma distribution $N(D)$ with parameters n_0, μ and λ, the corresponding droplet mass distribution $f(x)$ has the form (with droplet mass in grams, and considering the water density ρ_w=1):

$$f(x) = N(D)\left|\frac{dD}{dx}\right| = \frac{2n_0\left(\frac{6}{\pi}\right)^{(\mu-2)/3} x^{(\mu-2)/3} e^{-\lambda\left(\frac{6x}{\pi}\right)^{1/3}}}{\pi} \tag{27}$$

Then, the mass distribution for the bin microphysical model must be initialized from Eq. (27).

4. Rainshaft model setup and simulation results

The performance of the three-moment parameterization was tested within a horizontally homogeneous environment (rainshaft model). Our computational domain is an 8 km height vertical column, discretized with 80 grid points with a spacing of Δz = 100 m, and the time step was set equal to Δt = 1 s. This simplified setup is very useful to evaluate microphysical processes and has been used by other authors (Seifert and Beheng, 2001; Ziemer and Wacker, 2014).

The only microphysical processes considered in our study are sedimentation and collision-coalescence, with the configurations SBM-S, SBM-SC, M3-S, M3-SC and M2-S (see Table I for the definitions).

Table I. Configurations of the three-moment and two-moment parameterizations, and the spectral bin microphysics model.

Configuration	Description
SBM-S	Spectral-bin microphysics with sedimentation.
SBM-SC	Spectral-bin microphysics with sedimentation and collision-coalescence.
M3-S	Three-moment (M3) parameterization scheme with sedimentation determining μ.
M3-SC	Three-moment (M3) parameterization scheme with sedimentation and collision-coalescence determining μ.
M2-S	Two-moment (M2) parameterization scheme with sedimentation and a fixed value of μ.

4.1. Pure sedimentation case

The performance of three-moment schemes for pure sedimentation was analyzed in previous papers by Milbrandt and Yau (2005a), Milbrandt and McTaggart-Cowan (2010), and Ziemer and Wacker (2014). In this section, we also perform a comparison between M3-S, M2-S, and SBM-S before addressing the combined influence of collision-coalescence and sedimentation processes. For all the simulations, an initial 1.5 km thickness maritime cloud (which lies between 6000 and 7500 m) was assumed. Three different initial configurations were considered (with initial parameters taken from Ziemer and Wacker [2014]), with a liquid water content of L_{wc} = 5 × 10^{-7} g cm^{-3}, and a cloud droplet number concentration of N_0 = 3 × 10^{-3} cm^{-3}. Only the reflectivity was varied (see values in Table II) in order to obtain different initial distributions with different shape parameters for the three schemes (two-moment, three-moment and the bin-scheme).

The shape parameters μ calculated from these initial configurations were found equal to 0, 0.5, and

Table II. Initial conditions for the pure sedimentation case. For the three simulations, the liquid water content $L_{wc} = 5 \times 10^{-7}$ g cm^{-3} and the drop concentration $N_0 = 3 \times 10^{-3}$ cm^{-3} remain the same. The reflectivity was varied to obtain different initial gamma distribution parameters (cases 0, I and II from Table 5 of Ziemer and Wacker [2014]).

Z (cm^3)	Shape parameter (μ)	n_0	λ
6.0793×10^{-9}	0	7.9840×10^{-2}	26.6134
3.7257×10^{-9}	0.5	6.8793×10^{-1}	34.5475
9.1052×10^{-10}	4.8773	1.7501×10^{7}	100.0092

4.8773, respectively (see Table II), and serve us to initialize both the bin and three-moment parameterization schemes, and as the shape parameter (that has been fixed to these values during the entire simulations) for the two-moment parameterization scheme.

The results obtained for the three experiments (with $\mu = 0, 0.5$, and 4.8773) are displayed in Figures 1, 2, and 3 for three different times (200, 400, and 600 s). For the three experiments, the prognostic moments droplet concentration N, liquid water content L_{wc}, and reflectivity Z for the M3-S model, perform much better than the M2-S model, which has a fixed shape parameter.

For $\mu = 0$ there is a good coincidence between the three-moment and bin schemes for the prognostic moments liquid water content and reflectivity. However, the three-moment scheme slightly overestimates the maximum value for droplet number concentration at all times. For that case ($\mu = 0$), the two-moment scheme overestimates the droplet concentration and underestimates the prognostic moments liquid water content and the reflectivity.

For the second experiment (with shape parameter $\mu = 0.5$, Fig. 2), the M3-S model seems to slightly overestimate the maximum value for the number concentration at t = 600 s, but there is a good match between the three-moment and the spectral bin microphysical schemes for the prognostic moments liquid water content and the reflectivity. For the M2-S model, on the other hand, there is a marked underestimation of the prognostic moments liquid water content (L_{wc}) and reflectivity *(Z)*, and an overestimation of the prognostic moment number concentration.

For the case with an initial distribution with $\mu = 4.8773$, we saw that all the prognostic moments were well captured by the three-moment scheme. The M2-S model slightly underestimated the radar reflectivity at t = 600 s. We can conclude that the M3-S model, for all the prognostic moments (N, L, and Z) performs very well for narrower distributions (with $\mu = 0.5$ and 4.8773) and outperforms the two-moment parameterization scheme.

For the two-moment scheme, the liquid water content L_{wc} and reflectivity Z sediment faster than the M_0. This is confirmed by the medium radius vertical profile, with much larger values than the reference spectral model. For the three-moment scheme, on the other hand, a good coincidence between the mean radius profile for the spectral reference and the parameterization was obtained for different values of the initial shape parameter of the DSD

As can be observed in Figures 4, 5, and 6, both the two-moment and three-moment schemes produce a size sorting effect; however, the two-moment scheme is not very accurate at reproducing the medium radius profile, while the three-moment scheme performs very well on predicting the medium radius at all heights for the three cases (with $\mu = 0, 0.5$ and 4.8773), for all simulation times.

The cause of this discrepancy for two-moment schemes was already discussed in previous studies and outlined in the introduction (e.g., Milbrandt and MacTaggart-Cowan, 2010), and has its origin in the fact that for a scheme with a fixed value μ, the ratio of the moment-weighted sedimentation velocities (which is actually a function of the shape parameter) is always positive and larger than 1. The fact that a good correspondence was obtained between the three-moment and the spectral reference solution confirms that three-moment schemes give a physically based and more complete representation of the sedimentation processes.

Vertical profiles of shape parameter μ for three times (200, 400, and 600 s), and for three different initial values ($\mu = 0$, 0.5, and 4.8773) obtained from the M3-S model, are compared with those from SBM-S, which serves as a benchmark (Figs. 7, 8, and 9). The figures were obtained for cloud droplet concentrations larger than 10^{-6} cm^{-3}.

For this comparison, it is assumed that the DSD for the bin model (which evolves without restric-

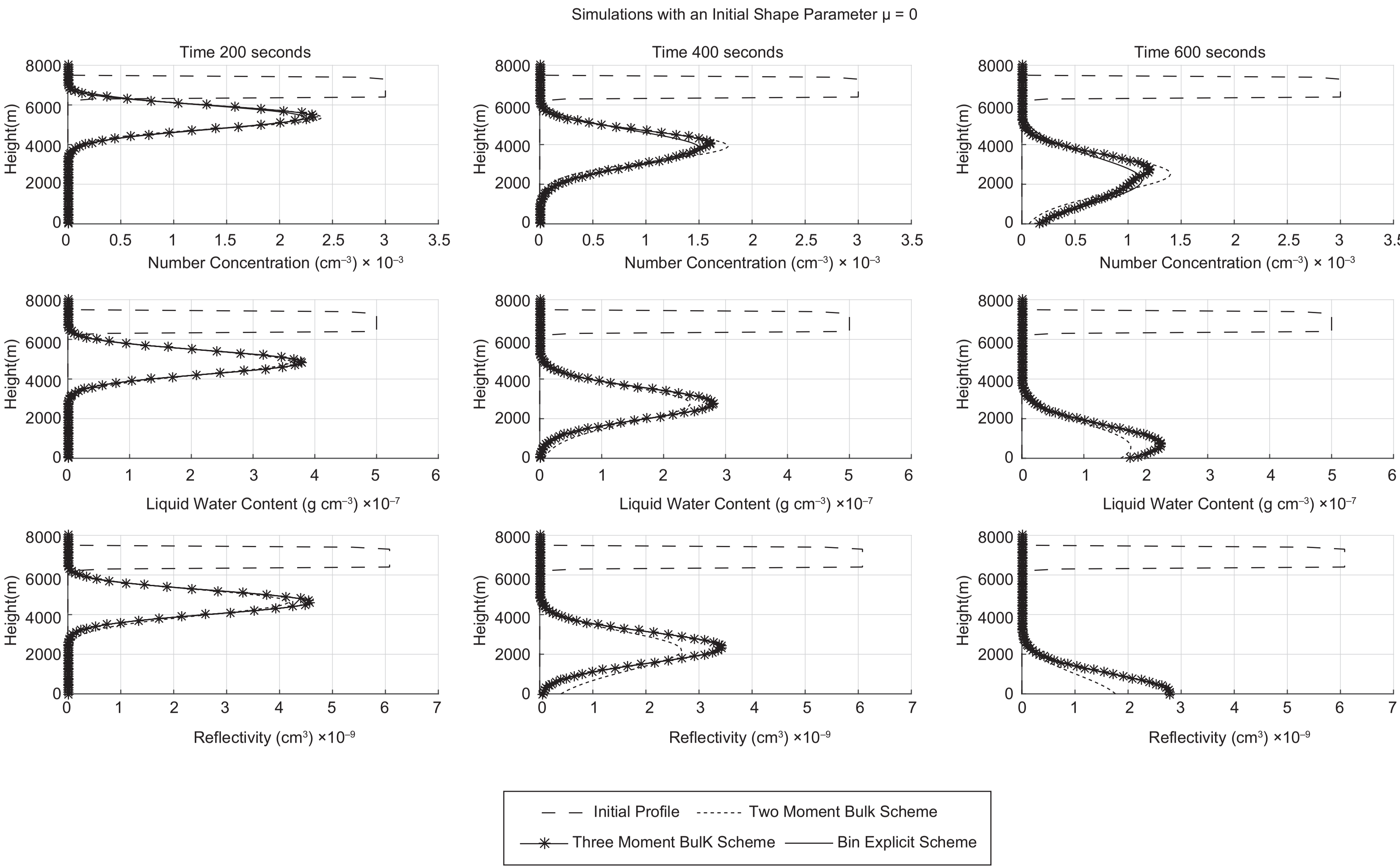

Fig. 1. Vertical profiles of droplet concentration (N), liquid water content (L_{wc}), and reflectivity (Z) for the two- and three-moment parameterization schemes, and the explicit reference solution (continuous line). The results were obtained for the case with an initial shape parameter $\mu_{\mathrm{init}} = 0$, and are displayed for three times (200, 400 and 600 s).

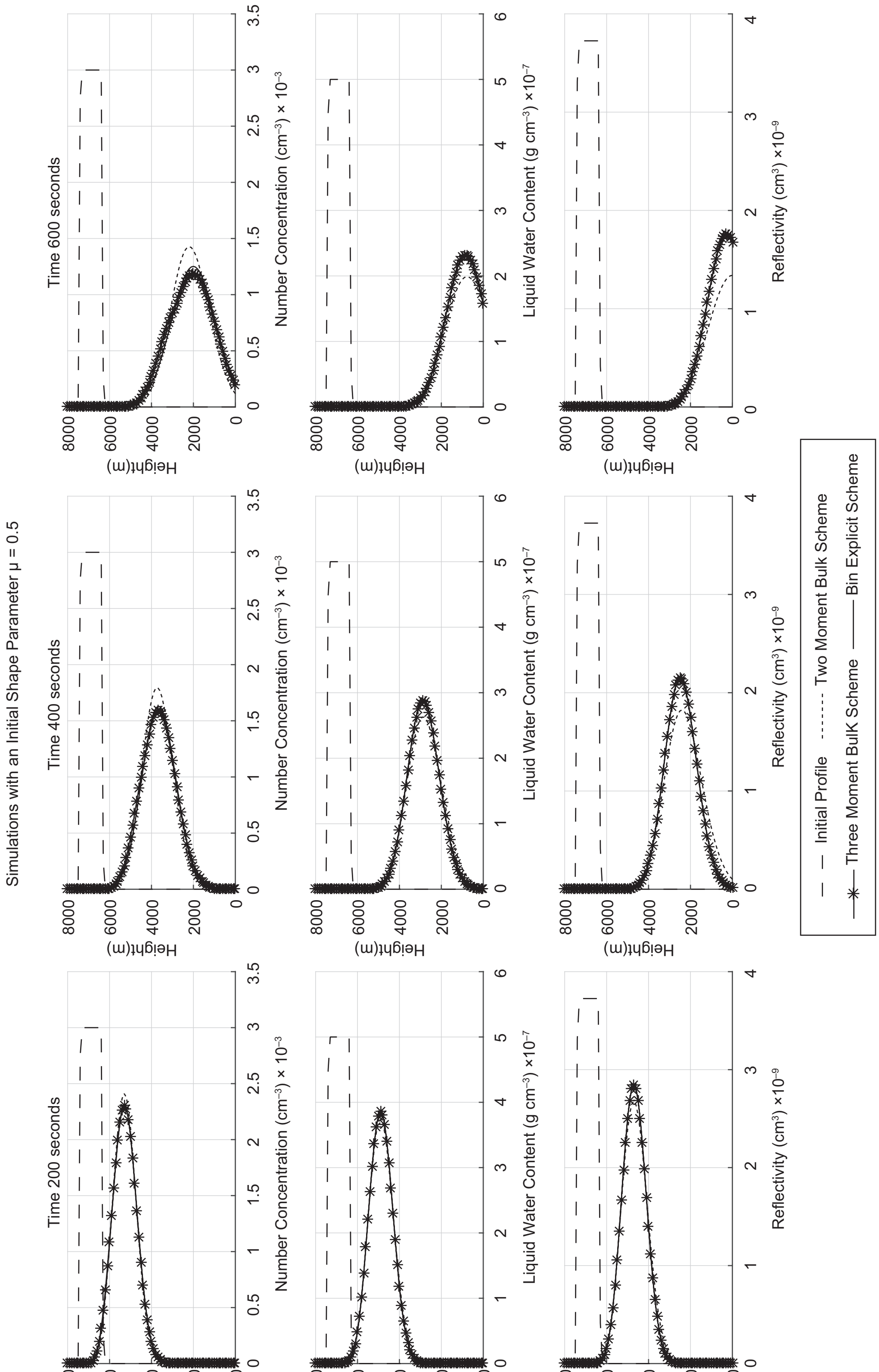

Fig. 2. Same as in Figure 1, but for the case with an initial shape parameter $\mu = 0.5$.

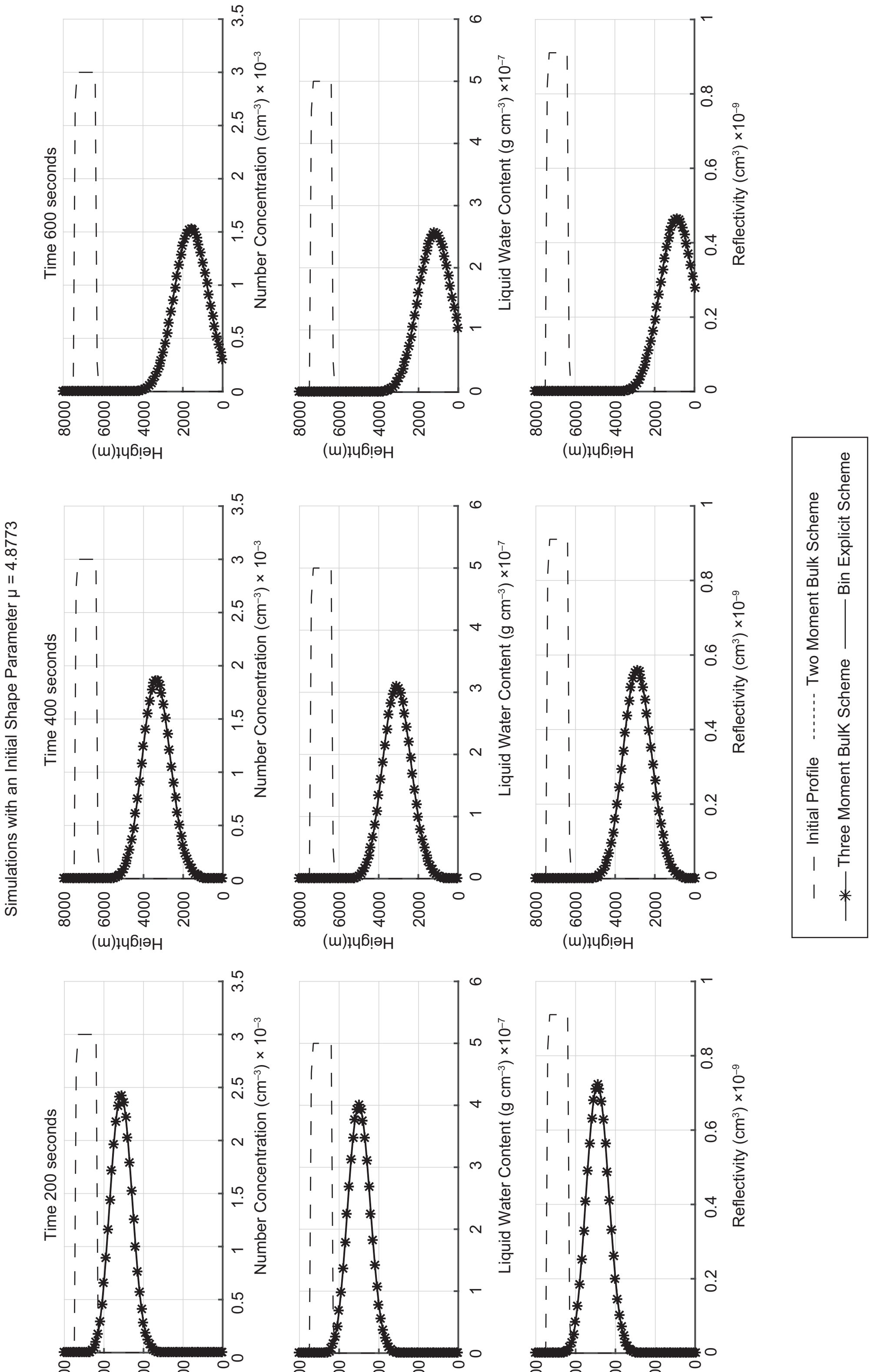

Fig 3. Same as in Figure 1, but for the case with an initial shape parameter $\mu = 4.8773$.

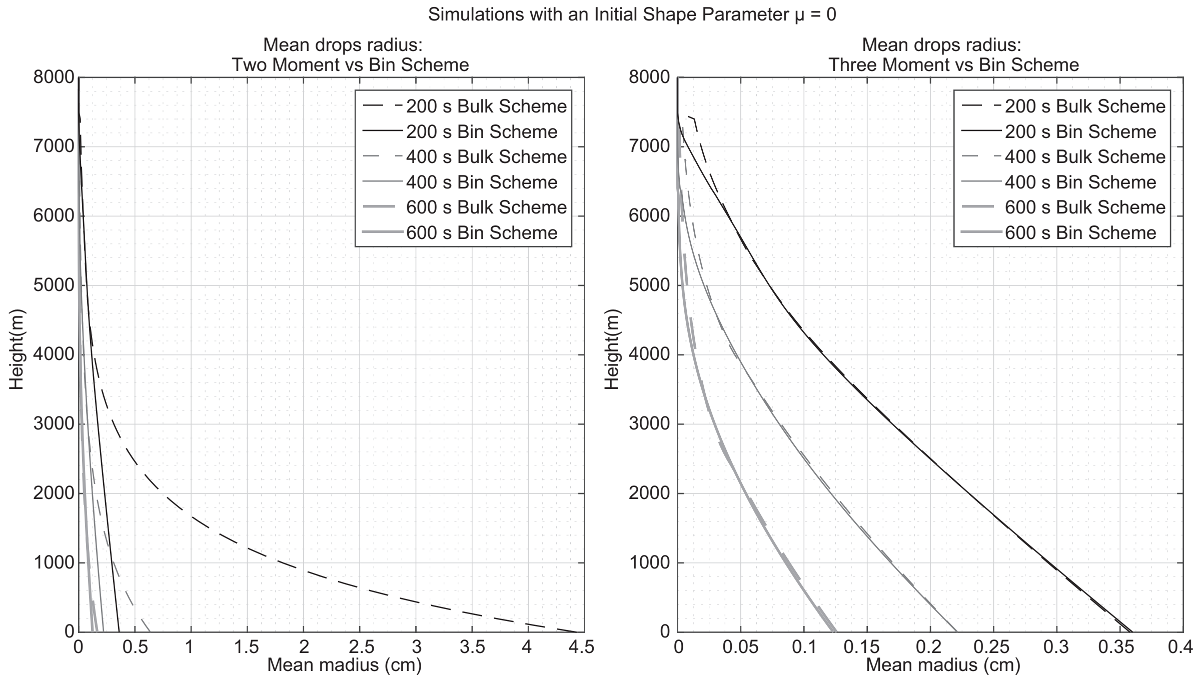

Fig. 4. Mean radius vertical profiles obtained from the two- and three-moments parameterization schemes, and the explicit reference solution (continuous line). The results were obtained for the case with an initial shape parameter $\mu = 0$, and are displayed for three times (200, 400 and 600 s).

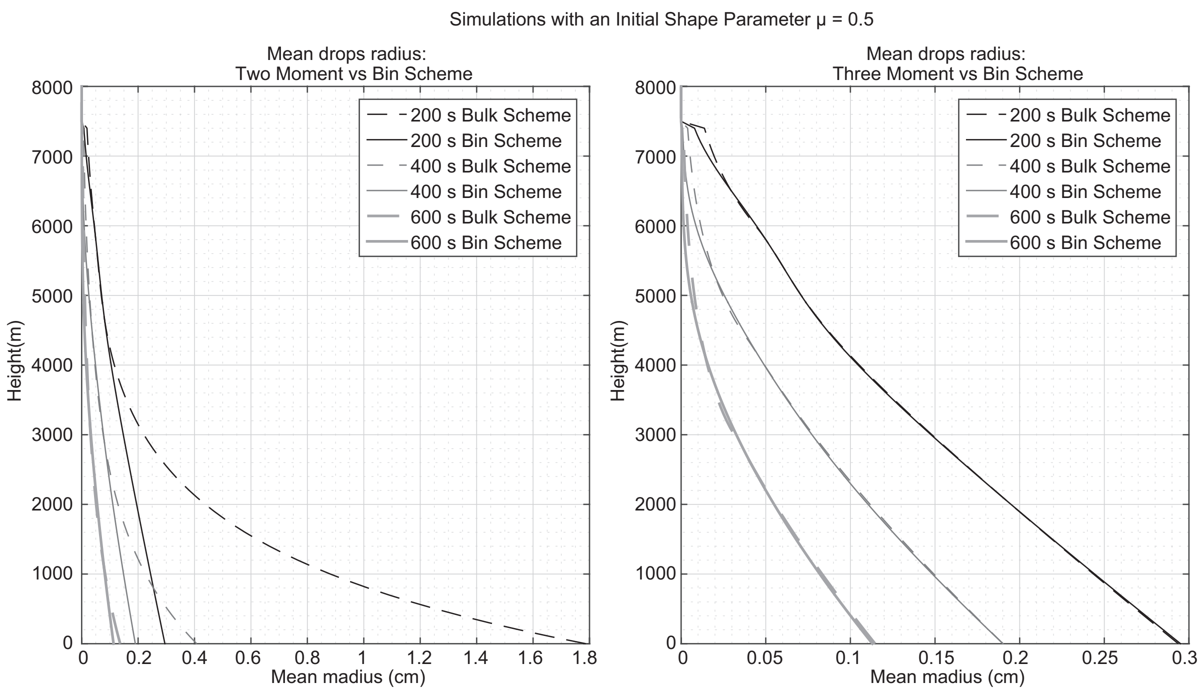

Fig. 5. Same as in Figure 4, but for the case with an initial shape parameter $\mu = 0.5$.

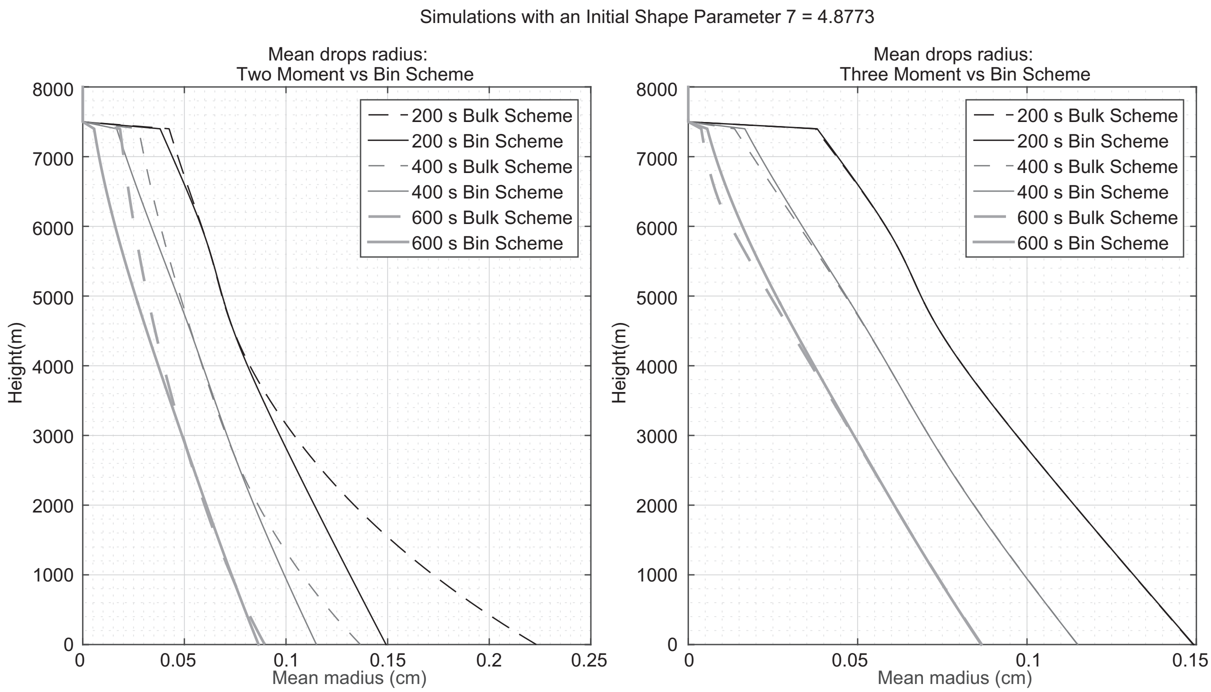

Fig. 6. Same as in Figure 4, but for the case with an initial shape parameter μ = 4.8773.

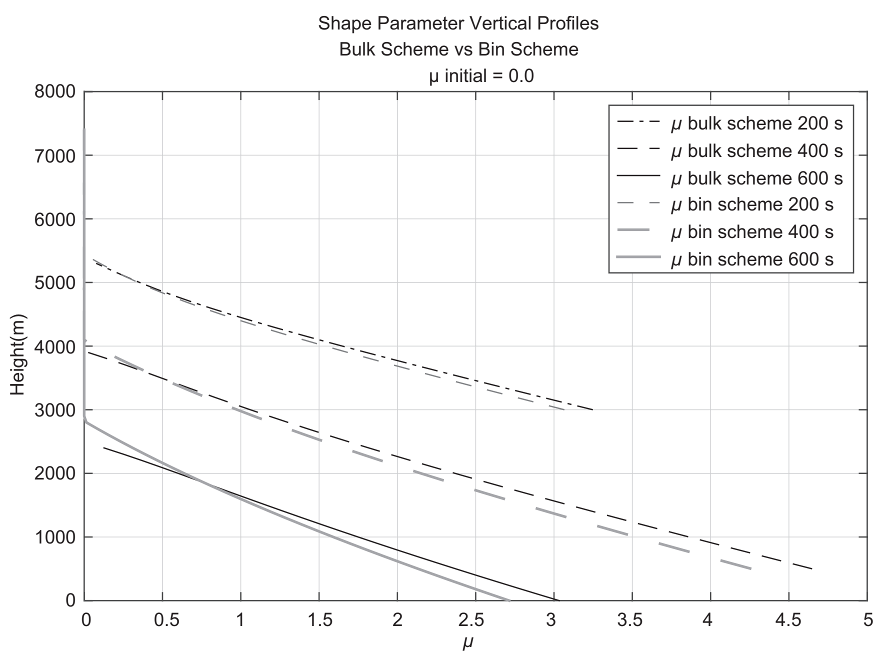

Fig. 7. Vertical profiles of the shape parameter for the bulk (thick lines) and bin schemes (thin lines) for three times (200, 400 and 600 s). The results were obtained for the case with an initial shape parameter μ = 0.

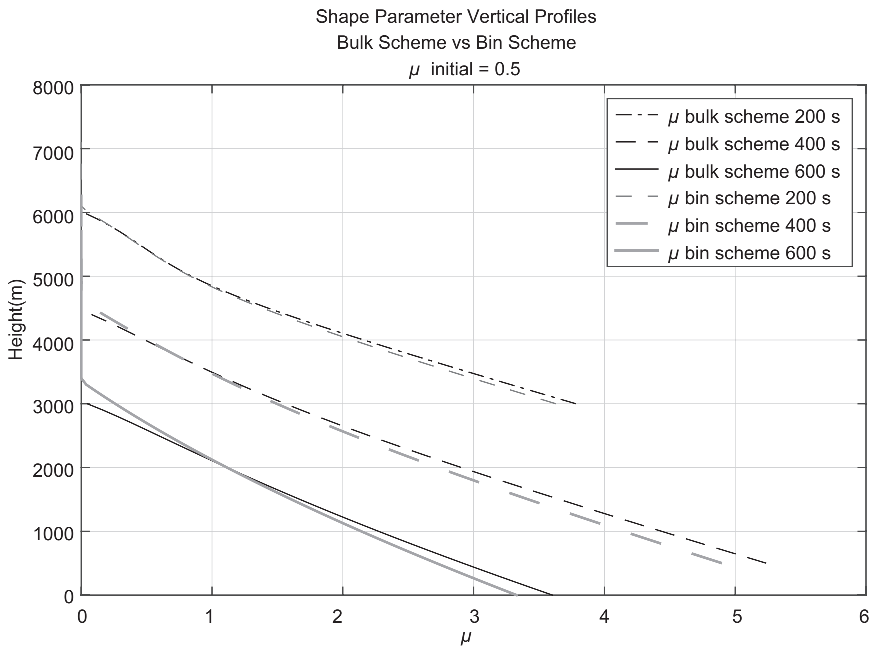

Fig. 8. Same as in Figure 7, but for the case with an initial shape parameter $\mu = 0.5$.

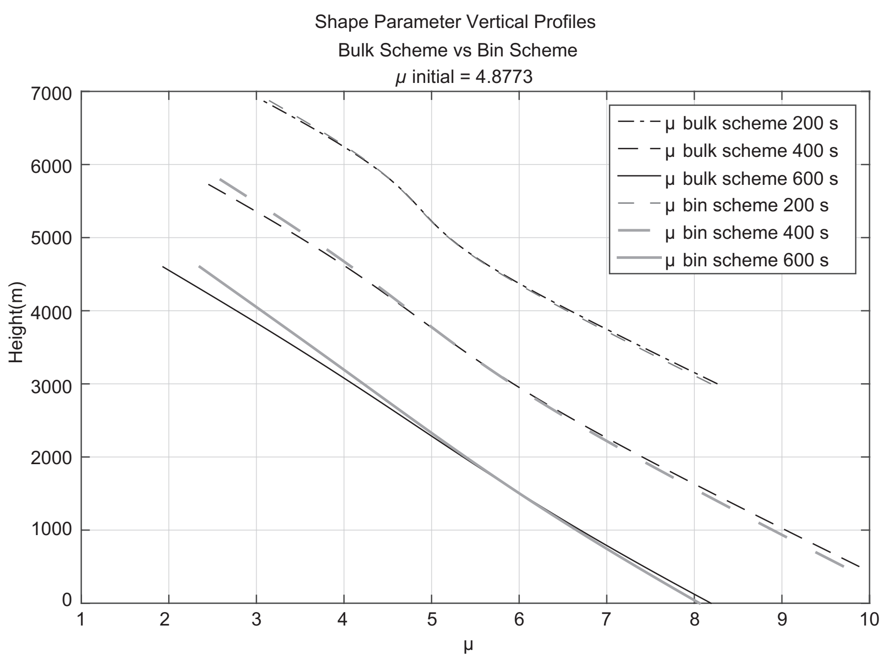

Fig. 9. Same as in Figure 7, but for the case with an initial shape parameter $\mu = 4.8773$.

tions for the bin microphysical model) follows a gamma distribution (Paukert et al., 2019). As can be observed, the shape parameter profiles from the parameterized model follow very closely the shape parameter obtained from the bin model under the assumption that the DSD is gamma. This leads us to the conclusion that the gamma distribution works well as an approximation of the DSD for the sedimentation case and that the bulk M3-S model is able to capture the evolution of the shape parameter.

To assess the impact of the sedimentation process on the DSD shape parameter, contour plots for two different initial values of the shape parameter (μ = 0.5 and 4.8773) were calculated (Figs. 10 and 11). As can be checked in these figures, there is an increase in the shape parameter as cloud height decreases, and consequently (as the shape parameter μ is related to the relative dispersion ε of the DSD from the relation $\mu = \varepsilon^{-2} - 1$) a decrease of the relative dispersion. The increase of μ is a result of size sorting, which tends to make DSD much narrower. For the two-moment scheme (with a constant value of the shape parameter), there is an excess size sorting and consequently an overestimation of the mean radius (Fig. 4, left panel). For the three-moment scheme, the DSD tends to be narrower, and the model reproduces quite accurately the mean radii obtained with the explicit model. We can conclude that the M3-S model (with variable shape parameter) captures well the narrowing size distribution resulting from size sorting (Fig. 4, right panel).

4.2 Combined effect of sedimentation and collision coalescence

Two simulations were performed with the configurations SBM-SC (spectral-bin microphysics with sedimentation and collision-coalescence) and M3-SC (three-moment parameterization scheme with sedimentation and collision-coalescence determining μ), the former serving as a benchmark. As for the pure sedimentation case, a 1.5 km thickness maritime cloud (which lies between 6000 and 7500 m) was assumed, with a cloud liquid water content of $L_{wc} = 2 \times 10^{-6}$ g cm^{-3}, a cloud drop number concentration of $N_{0c} = 100$ cm^{-3}, and a reflectivity of $Z_{0c} = 3.8213 \times 10^{-13}$ cm^3 (see Table III). For this combination of distribution moments, the initial value of the shape parameter was found equal to $\mu = 5.99$. For the two experiments, the simulation time was set equal to $t = 1800$ sec.

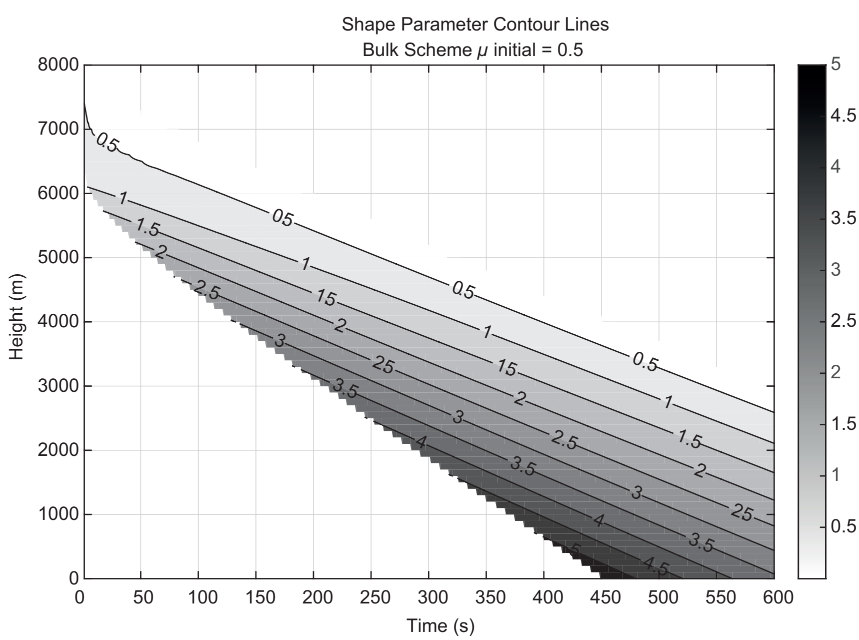

Fig. 10. Contour shape parameter lines for the bulk scheme for an initial shape parameter $\mu = 0.5$, for the pure sedimentation case.

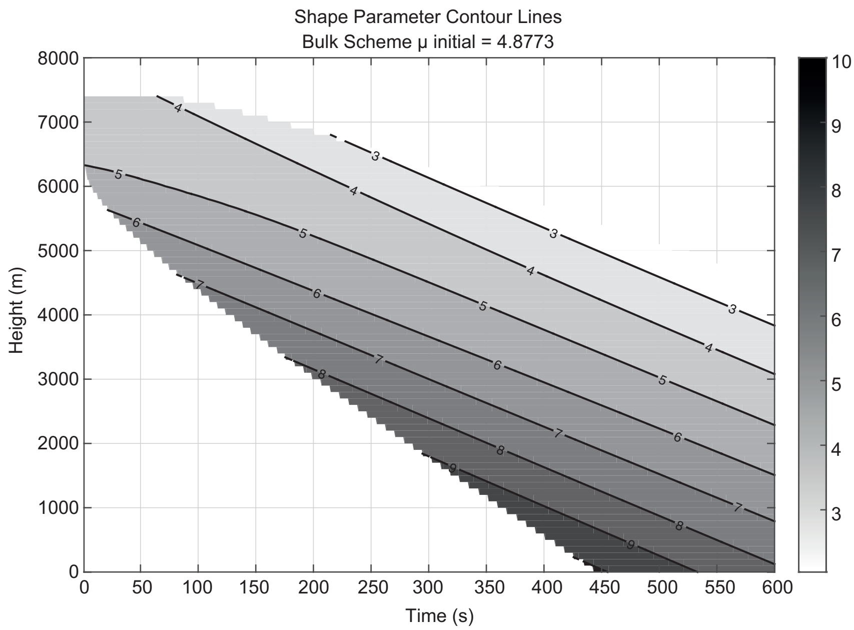

Fig. 11. Same as in Figure 10, but for an initial shape parameter $\mu = 4.8773$.

Table III. Initial conditions for the simulations with combined effect of sedimentation and collision-coalescence.

Symbol	Description	Values
L_{wc}	Initial cloud liquid water content	2×10^{-6} g cm^{-3}
N_{0c}	Initial cloud droplet number concentration	10^2 cm^{-3}
Z_{0c}	Initial cloud reflectivity	3.8213×10^{-13} cm^3

The comparison between the SBM-SC and M3-SC cases was performed by plotting the evolution in time of the prognostic moments (concentration, liquid water content, and reflectivity). As can be observed in Figures 12 and 13, in general, there is a good agreement between the parameterized and the bin microphysics models.

The time-height distributions for cloud water drop number concentrations, cloud liquid water content, and radar reflectivity (Fig. 12) are very similar. For all cases, the slope in all the figures indicates that the sedimentation process is activated, and the hydrometeors (cloud and rain drops) are falling to the ground. At $t = 0$, we have the same distribution, and constant values between 6000 and 7500 m. As time evolves, the drop number concentration decreases due to the combined effect of the collision-coalescence and sedimentation processes.

However, a more critical analysis of Figs. 12 and 13 reveals some differences between the SBM-SC and the M3-SC models. Compared to SBM-SC, the three-moment scheme exhibits a slightly larger coalescence rate, a fact that becomes clear when observing the values of rain number concentration and liquid water content at the same time. For example, at $t = 600$ s, the parameterized scheme exhibits values of rain number concentration larger than 0.20 cm^{-3}, while for the explicit model, the concentration values are in the order of 0.14 cm^{-3}. Accordingly, the same behavior is observed for the rain liquid water content, with values of 5.5×10^{-9} g cm^{-3} and 5×10^{-9} g cm^{-3} for the M3-SC and the SBM-SC models, respectively.

These results for rainwater are consistent with a faster rate of decrease in cloud droplet concentration for the parameterized model. For example, at $t = 1000$ s for the explicit model, we can find cloud droplet concentrations as large as 90 cm^{-3} at 3400 m, while for the parameterized model cloud droplet concentrations are smaller than 90 cm^{-3} at all cloud levels.

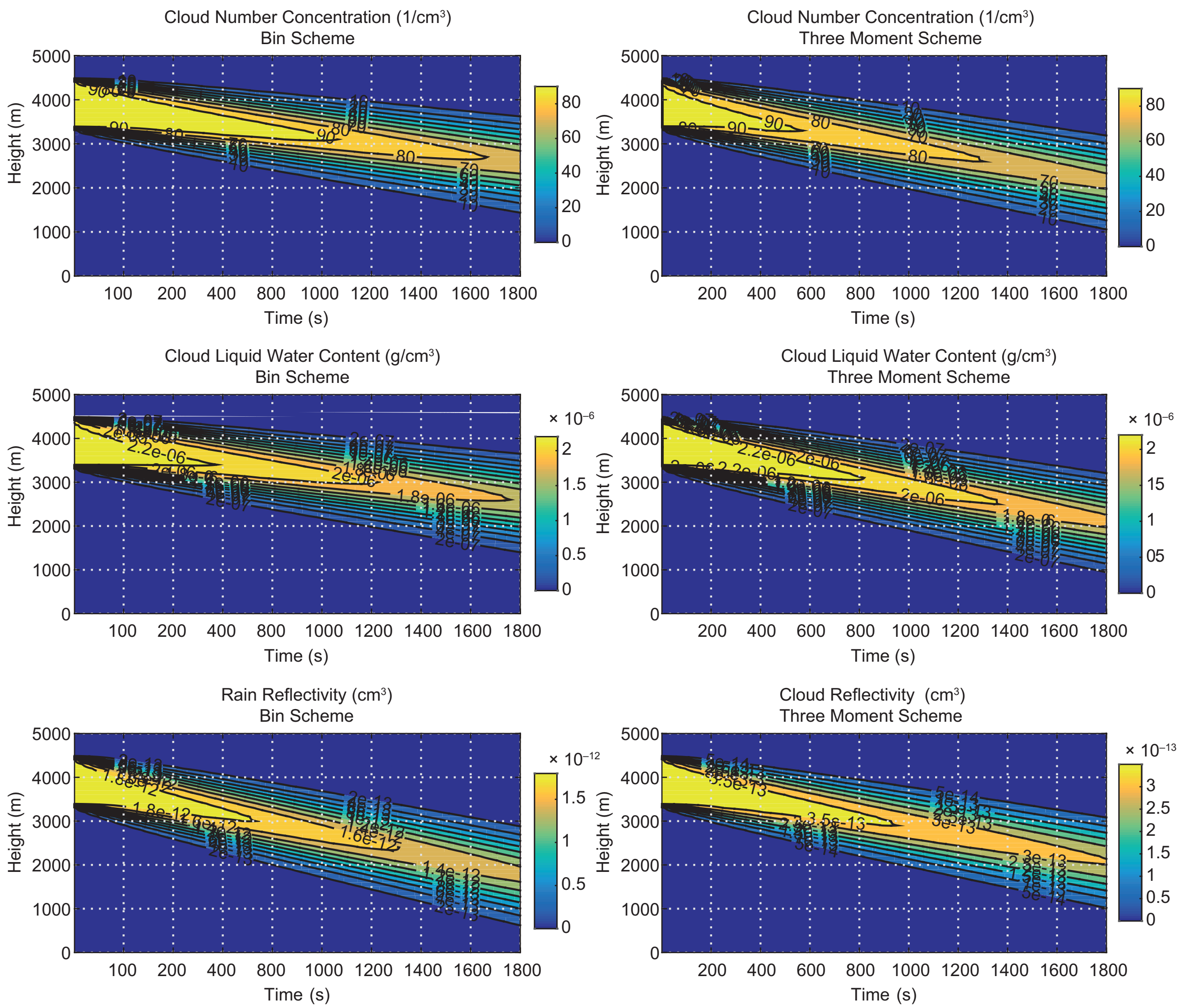

Fig. 12. Prognostic moments for cloud droplets. The left column is from simulation with the bin-microphysics scheme, and the right column is from simulation with the three-moment parameterized scheme. The top row is the droplet number concentration (N) in cm^{-3}, the second row is the liquid water content (L_{wc}) in g cm^{-3}, and the third row is the reflectivity (Z) in cm^3.

For cloud liquid water content and cloud reflectivity, in general, the three-moment parameterized model emulates very well the results obtained with the bin model, especially for cloud water reflectivity, with very similar time-height profiles for the two models.

Figures 12 and 13 show that the results obtained with the three-moment scheme for this case (with the combined effect of sedimentation and collision coalescence) are found to agree well with those obtained with the explicit model. Some differences are unavoidable, due to the complexity of the schemes and the incorporation of other processes. Overall, the model reproduces quite accurately the results obtained with the explicit model.

5. Discussion and conclusions

In this paper, a bulk three-moment parameterization scheme incorporating sedimentation and collision-coalescence was developed and evaluated.

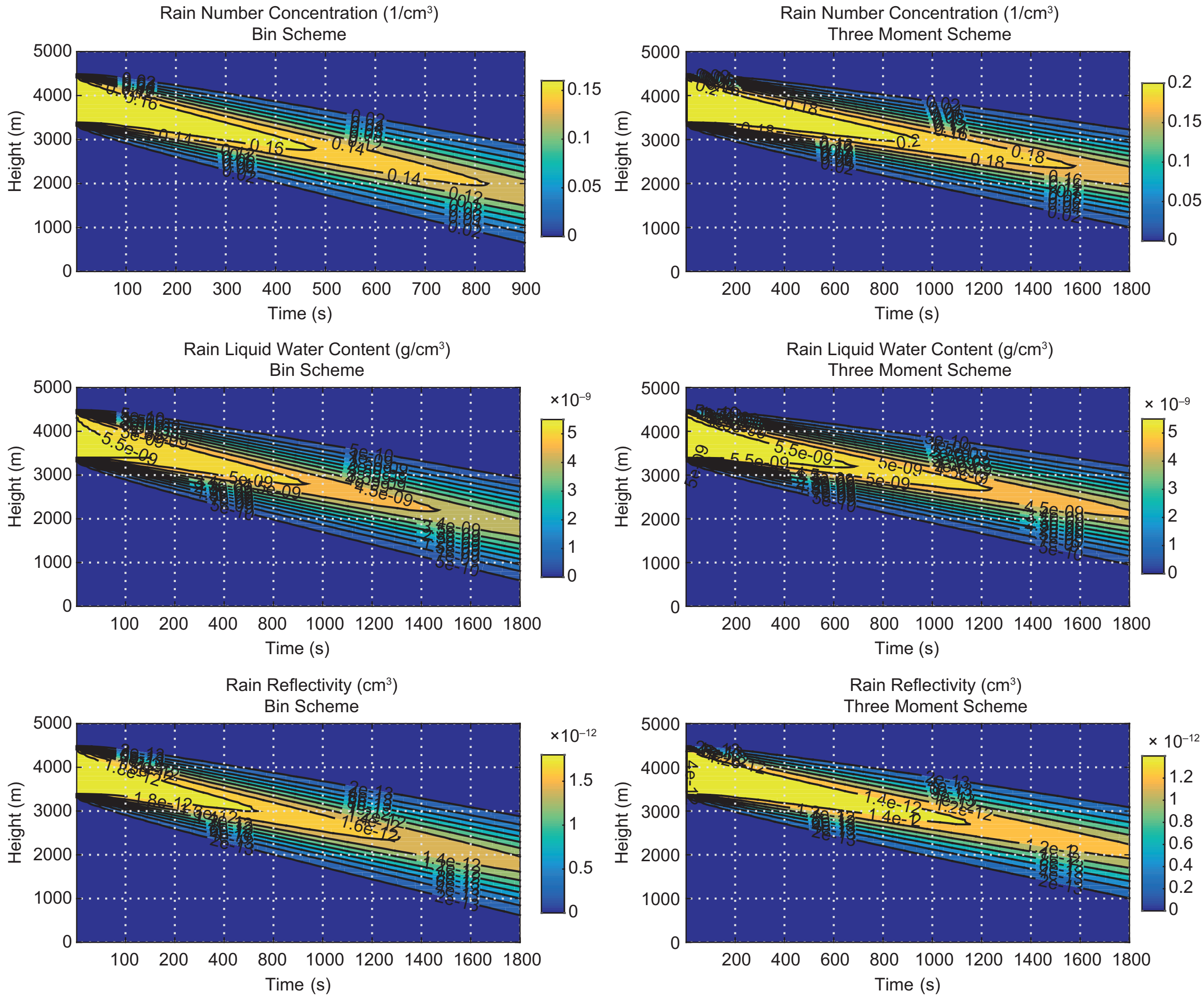

Fig. 13. Prognostic moments for raindrops. The left column is from simulation with the bin-microphysics scheme, and the right column is from simulation with the three-moment parameterized scheme. The top row is the rain number concentration (N) in cm^{-3}, the second row is the liquid water content (L_{wr}) in g cm^{-3}, and the third row is the reflectivity (Z) in cm^3.

The performance of the parameterized scheme was assessed through a detailed comparison with a bin microphysical scheme within a one-dimensional kinematic setting. For the comparison, the predicted moments were number density N, liquid water content L_{wc}, and radar reflectivity Z.

In our simulations, for the pure sedimentation case, results from the three-moment parameterized scheme are found to agree well with those from simulation using the bin microphysical scheme (for the three predicted moments) for initial values of the shape parameter $\mu = 0.5$ and 4.8773. For $\mu = 0$, the three-moment scheme slightly overestimates the maximum value for droplet concentration at all times. Better results are obtained for narrower initial distributions (with larger values of the shape parameter). The results obtained justified the adoption of the new procedure for calculating the shape parameter μ outlined in Paukert et al. (2019).

The mean radius vertical profiles calculated from the three-moment parameterized scheme match very well those obtained from simulations using the bin microphysical scheme, confirming (as discussed previously by Milbrandt and Yau [2005a], Milbrandt and McTaggart-Cowan [2010], and Ziemer and Wacker [2014]), that three-moment parameterization schemes outperform the two-moment schemes, and that the inclusion of a third moment in order to predict μ gives a more realistic description of the DSD evolution due to sedimentation.

When the collision-coalescence process is incorporated, overall, results from the three-moment scheme are found to agree qualitatively well with those obtained from simulation using the explicit scheme. However, the onset of precipitation occurs earlier in the M3-SC model, with a clear overestimation of the raindrop number concentration and the rain liquid water content.

The small differences between the prognostic moments profiles for the SBM-SC and the M3-SC models are clearly a result of the incorporation of the collision-coalescence process. Overall, results from the three-moment parameterized scheme are found to agree well with those from simulations using the bin microphysical scheme. However, we were unable to find the level of proximity to the reference solution that was obtained for the pure sedimentation case.

This can be explained by the complexity of the Kessler-type parameterizations that involved six prognostic moments (N_c, Q_c, Z_c, and N_r, Q_r, Z_r) and three microphysical processes (autoconversion, accretion, and self-collection). Also, when developing parameterizations for the collection process (Cohard and Pinty, 2000), the polynomial form of the collection kernel developed by Long (1974) is considered to obtain analytical expressions for the integrals of the KCE (in the form of gamma functions). Then, the results will differ from those obtained from the integration of the KCE with the hydrodynamic kernel Eq. (24).

A further effort to improve the analytical approach (that uses an approximated form of the collection kernel) could lie in the adoption of the machine learning (ML) approach, which was used for the autoconversion process with good results by Alfonso and Zamora (2021). For the Kessler-type parameterizations, it could be extended in order to include the processes of accretion and self-collection, and embedded into a dynamic framework in order to check the performance through a direct comparison with a spectral model.

Acknowledgments

Lainer Donet was supported by a grant from Mexico's Consejo Nacional de Ciencia y Tecnología (CONACyT). This paper was also partially funded by a grant from CONACyT (SEP-CONACyT CB-284482).

References

Alfonso L, Zamora JM. 2021. A two-moment machine learning parameterization of the autoconversion process. Atmospheric Research 249: 105269. https://doi.org/10.1016/j.atmosres.2020.105269

Beheng KD. 2010. The evolution of raindrop spectra: A review of microphysical essentials. Rainfall. State of the Science 191: 29-48. https://doi.org/10.1029/2010GM000957

Berry EX. 1967. Cloud droplet growth by collection. Journal of the Atmospheric Sciences 24: 688-701. https://doi.org/10.1175/1520-0469(1967)024<0688:CDGBC>2.0.CO;2

Bott A. 1998. A flux method for the numerical solution of the stochastic collection equation. Journal of the Atmospheric Sciences 55: 2284-2293. https://doi.org/10.1175/1520-0469(1998)055<2284:AFMFTN>2.0.CO;2

Cohard, JM, Pinty JP. 2000. A comprehensive two-moment warm microphysical bulk scheme. II: 2D experiments with a non-hydrostatic model. Quarterly Journal of the Royal Meteorological Society 126: 1843-1859. https://doi.org/10.1002/qj.49712656614

Dawson DT, Mansell ER, Jung Y, Wicker LJ, Kumjian MR, Xue M. 2014. Low-level Z DR signatures in supercell forward flanks: The role of size sorting and melting of hail. Journal of the Atmospheric Sciences 71: 276-299.

Ferrier BS. 1994. A double-moment multiple-phase four-class bulk ice scheme. Part I: Description. Journal of the Atmospheric Sciences 51: 249-280.

Gunn R, Kinzer GD. 1949. The terminal velocity of fall for water droplets in stagnant air. Journal of Meteorology 6: 243-248.

Kessler E. 1969. On the distribution and continuity of water substance in atmospheric circulations. In: On the distribution and continuity of water substance in atmospheric circulations. Meteorological Monographs, vol. 10. American Meteorological Society, Boston, MA, 1-84. https://doi.org/10.1007/978-1-935704-36-2_1

Khain AP, Beheng KD, Heymsfield A, Korolev A, Krichak SO, Levin Z, Pinsky M, Phillips V, Prabhakaran T, Teller A, van den Heever SC, Yano JI. 2015. Representation of microphysical processes in cloud-resolving models: Spectral (bin) microphysics versus bulk parameterization. Reviews of Geophysics 53: 247-322. https://doi.org/10.1002/2014RG000468

Khairoutdinov M, Kogan Y. 2000. A new cloud physics parameterization in a large-eddy simulation model of marine stratocumulus. Monthly Weather Review 128: 229-243. https://doi.org/10.1175/1520-0493(2000)128<0229:ANCPPI>2.0.CO;2

Hall W. 1980. A detailed microphysical model within a two-dimensional dynamic framework: Model description and preliminary results. Journal of the Atmospheric Sciences 37: 2486-2507. https://doi.org/10.1175/1520-0469(1980)037<2486:ADMMWA>2.0.CO;2

Lee H, Baik JJ. 2017. A physically based autoconversion parameterization. Journal of the Atmospheric Sciences 74: 1599-1616. https://doi.org/10.1175/JAS-D-16-0207.1

Lim KSS, Hong SY. 2010. Development of an effective double-moment cloud microphysics scheme with prognostic cloud condensation nuclei (CCN) for weather and climate models. Monthly Weather Review 138: 1587-1612. https://doi.org/10.1175/2009MWR2968.1

Loftus AM, Cotton WR, Carrió GG. 2014. A triple-moment hail bulk microphysics scheme. Part I: Description and initial evaluation. Atmospheric Research 149: 35-57. https://doi.org/10.1016/j.atmosres.2014.05.013

Long AB. 1974. Solutions to the droplet collection equation for polynomial kernels. Journal of the Atmospheric Sciences 31: 1040–1052. https://doi.org/10.1175/1520-0469(1974)031<1040:STTDCE>2.0.CO;2

Milbrandt JA, Yau MK. 2005a. A multimoment bulk microphysics parameterization. Part I: Analysis of the role of the spectral shape parameter. Journal of the Atmospheric Sciences 62: 3051-3064. https://doi.org/10.1175/JAS3534.1

Milbrandt JA, Yau MK. 2005b. A multimoment bulk microphysics parameterization. Part II: A proposed three-moment closure and scheme description. Journal of the Atmospheric Sciences 62: 3065-3081. https://doi.org/10.1175/JAS3535.1

Milbrandt JA, McTaggart-Cowan R. 2010. Sedimentation-induced errors in bulk microphysics schemes. Journal of the Atmospheric Sciences 67: 3931-3948. https://doi.org/10.1175/2010JAS3541.1

Morrison HC, Curry JA, Khvorostyanov VI. 2005. A new double-moment microphysics parameterization for application in cloud and climate models. Part I: Description. Journal of the Atmospheric Sciences 62: 1665-1677. https://doi.org/10.1175/JAS3446.1

Morrison H, Thompson G, Tatarskii V. 2009. Impact of cloud microphysics on the development of trailing stratiform precipitation in a simulated squall line: Comparison of one- and two-moment schemes. Monthly Weather Review 137: 991-1007. https://doi.org/10.1175/2008MWR2556.1

Murakami M. 1990. Numerical modeling of dynamical and microphysical evolution of an isolated convective cloud. Journal of the Meteorological Society of Japan. Ser. II 68: 107-128. https://doi.org/10.2151/jmsj1965.68.2_107

Naumann AK, Seifert A. 2016. Evolution of the shape of the raindrop size distribution in simulated shallow cumulus. Journal of the Atmospheric Sciences 73: 2279-2297. https://doi.org/10.1175/JAS-D-15-0263.1

Paukert M, Fan J, Rasch PJ, Morrison H, Milbrandt JA, Shpund J, Khain A. 2019. Three-moment representation of rain in a bulk microphysics model. Journal of Advances in Modeling Earth Systems 11: 257-277. https://doi.org/10.1029/2018MS001512

Press WH, Teukolsky SA, Vetterling WT, Flannery BP. 1992. Numerical recipes in Fortran 77. Fortran numerical recipes: The art of scientific computing (vol. 1). Cambridge University Press, New York.

Pruppacher H, Klett J. 1997. Microphysics of clouds and precipitation. Kluwer Academic Publishers, Dordrecht, 954 pp.

Reisner J, Rasmussen RM, Bruintjes RT. 1998. Explicit forecasting of supercooled liquid water in winter storms using the MM5 mesoscale model. Quarterly Journal of the Royal Meteorological Society 124: 1071-1107. https://doi.org/10.1002/qj.49712454804

Rogers RR, Yau MK. 1989. A Short Course in Cloud Physics. Pergamon Press 290.

Seifert A, Beheng KD. 2001. A double-moment parameterization for simulating autoconversion, accretion and selfcollection. Atmospheric Research 59-60: 265-281. https://doi.org/10.1016/S0169-8095(01)00126-0

Seifert A, Beheng KD. 2006. A two-moment cloud microphysics parameterization for mixed-phase clouds. Part 1: Model description. Meteorology and Atmospheric Physics 92: 45-66. https://doi.org/10.1007/s00703-005-0112-4

Shipway BJ, Hill AA. 2012. Diagnosis of systematic differences between multiple parametrizations of warm rain microphysics using a kinematic framework.

Quarterly Journal of the Royal Meteorological Society 138: 2196-2211. https://doi.org/10.1002/qj.1913

Straka JM. 2009. Cloud and precipitation microphysics: Principles and parameterizations. Cambridge University Press, Cambridge.

Szyrmer W, Laroche S, Zawadzki I. 2005. A microphysical bulk formulation based on scaling normalization of the particle size distribution. Part I: Description. Journal of the Atmospheric Sciences 62: 4206-4221. https://doi.org/10.1175/JAS3620.1

Wacker U, Seifert A. 2001. Evolution of rainwater profiles resulting from pure sedimentation: Spectral vs. parameterized description. Atmospheric Research 58: 19-39. https://doi.org/10.1016/S0169-8095(01)00081-3

Waldvogel A. 1974. The N_0 jump of raindrop spectra. Journal of the Atmospheric Sciences 31: 1067-1078. https://doi.org/10.1175/1520-0469(1974)031<1067:TJORS>2.0.CO;2

Watkins AP. 2005. The application of gamma and beta number size distributions to the modelling of sprays. In: Proceedings of the 20th ILASS-Europe Meeting. Orleans, France, 103-108.

Wood R, Blossey PN. 2005. Comments on “Comments on “Parameterization of the Autoconversion Process. Part I: Analytical Formulation of the Kessler-Type Parameterizations”. Journal of the Atmospheric Sciences 62: 3003-3006. https://doi.org/10.1175/JAS3524.1

Ziemer C, Wacker U. 2014. A Comparative study of B-, Γ- and log-normal distributions in a three-moment parameterization for drop sedimentation. Atmosphere 5: 484-517. https://doi.org/10.3390/atmos5030484

SUPPLEMENTARY MATERIAL

S1. Bulk parameterization of the collision-coalescence process: autoconversion, accretion and self-collection.

The three-moment bulk microphysical scheme uses a generalized form of the gamma distribution (Cohard and Pinty, 2000; Milbrandt and Yau, 2005):

$$f(D) = N_i \frac{\alpha_i}{\Gamma(1+\mu_i)} \lambda_i^{\alpha_i(1+\mu_i)} D^{\alpha_i(1+\mu_i)-1} \tag{S1}$$

$$\exp(-(\lambda_i D)^{\alpha_i}) \qquad [cm^{-4}], \qquad D > 0$$

The distribution in Eq. (S1) reduces to the more common three-parameter gamma distribution (Eq. [1]) by setting $\alpha_i = 1$. Then, from Eq. (S1) it can be found that the intercept in Eq. (1) is defined as:

$$n_0 = N_i \frac{\lambda_i^{(1+\mu_i)}}{\Gamma(1+\mu_i)} \tag{S2}$$

In Eq. (S1), the index i stands for cloud or rain. The drop size distribution is separated into two categories (cloud and rain) by a threshold diameter of $D = 82\ \mu$m for calculating the autoconversion rates. Cohard and Pinty (2000) defined two phases for the autoconversion process, the "initiation stage" and the "feeding stage". Autoconversion rates for drop number concentration and cloud water mixing ratio at the "initial stage" are parameterized in the form (Cohard and Pinty, 2000):

$$\frac{1}{2}\frac{\partial N_c}{\partial t}\bigg|_{auto} = -\frac{\partial N_r}{\partial t}\bigg|_{auto} = -3.5\times 10^9 \frac{\rho_a L}{\tau} \tag{S3}$$

$$\frac{\partial Q_c}{\partial t}\bigg|_{auto} = -\frac{\partial Q_r}{\partial t}\bigg|_{auto} = -\max\left(L/\tau, 0\right) \tag{S4}$$

In Eqs. (S2) and (S3),

$$L = 2.7\times 10^{-2} \rho_a r_c \left(\frac{1}{16}\times 10^{20} \sigma_c^{\ 3} D_c - 0.4\right)$$

and,

$$\tau = 3.7 \times \frac{1}{\rho_a r_c} \times \left(0.5\times 10^6 \sigma_c - 7.1\right)^{-1}$$

ρ_a is the density of air,

$$D_c = \left\{\frac{M_3}{M_0}\right\}^{1/3}$$

is the mean volume diameter, and is the standard deviation of the DSD. Accretion and self-collection must be limited or excluded during this stage. For the "feeding stage" (that starts when the condition $Q_r > 1.2L$ is fulfilled), the drop number concentration auto conversion rates are calculated from the equations:

$$-\frac{1}{2}\frac{\partial N_c}{\partial t}\bigg|_{auto} = \frac{\partial N_r}{\partial t}\bigg|_{auto} = \frac{N_r}{Q_r} \times \frac{\partial Q_r}{\partial t}\bigg|_{auto} \tag{S5}$$

When the collecting drop is greater than 100 μm in diameter the accretion rates are (Cohard and Pinty, 2000):

$$\frac{\partial N_c}{\partial t}\bigg|_{accr} = K_1 N_c N_r \left\{\frac{\Gamma\left((\mu_c+1)+3/\alpha_c\right)}{\Gamma(\mu_c+1)\lambda_c^3} + \frac{\Gamma\left((\mu_r+1)+3/\alpha_r\right)}{\Gamma(\mu_r+1)\lambda_r^3}\right\} \tag{S6}$$

$$\frac{\partial Q_c}{\partial t}\bigg|_{accr} = \frac{\pi}{6}\frac{\rho_w}{\rho_a} K_1 \frac{N_c N_r}{\lambda_c^3} \left\{\frac{\Gamma\left((\mu_c+1)+6/\alpha_c\right)}{\Gamma(\mu_c+1)\lambda_c^3} + \frac{\Gamma\left((\mu_c+1)+3/\alpha_c\right)}{\Gamma(\mu_c+1)} \times \frac{\Gamma\left((\mu_r+1)+3/\alpha_r\right)}{\Gamma(\mu_r+1)\lambda_r^3}\right\} \tag{S7}$$

where $K_1 = 3.03 \times 10^3\ m^{-3}\ s^{-1}$. And if the collecting drop is smaller than 100 μm in diameter:

$$\frac{\partial N_r}{\partial t}\bigg|_{accr} = K_2 N_c N_r \left\{\frac{\Gamma\left((\mu_c+1)+6/\alpha_c\right)}{\Gamma(\mu_c+1)\lambda_c^6} + \frac{\Gamma\left((\mu_r+1)+6/\alpha_r\right)}{\Gamma(\mu_r+1)\lambda_r^6}\right\} \tag{S8}$$

$$\frac{\partial Q_r}{\partial t}\bigg|_{accr} = \frac{\pi}{6}\frac{\rho_w}{\rho_a} K_2 \frac{N_c N_r}{\lambda_c^3} \left\{\frac{\Gamma\left((\mu_c+1)+9/\alpha_c\right)}{\Gamma(\mu_c+1)\lambda_c^6} + \frac{\Gamma\left((\mu_c+1)+3/\alpha_c\right)}{\Gamma(\mu_c+1)} \times \frac{\Gamma\left((\mu_r+1)+6/\alpha_r\right)}{\Gamma(\mu_r+1)\lambda_r^6}\right\} \tag{S9}$$

with $K_2 = 2.59 \times 10^{15}\ m^{-3}\ s^{-1}$. Finally, for self-collection we have the equations (when the collecting drop is greater/smaller than 100 μm, respectively):

$$\frac{\partial N_i}{\partial t}\bigg|_{self} = K_1 N_i^2 \frac{\Gamma\left(\nu_i + 3/\alpha_i\right)}{\Gamma(\nu_i)\lambda_i^3} \tag{S10}$$

$$\frac{\partial N_i}{\partial t}\bigg|_{self} = K_2 N_i^2 \frac{\Gamma\left(\nu_i + 6/\alpha_i\right)}{\Gamma(\nu_i)\lambda_i^6} \tag{S11}$$

In Eqs. (S9) and (S10), index i stands for cloud or rain, respectively.